J Mater Sci (2009) 44:639–646
DOI 10.1007/s10853-008-3061-8

Destabilization of cubic-stabilized zirconia electrolyte induced by boron oxide under reducing atmosphere

Haruo Kishimoto · Natsuko Sakai · Katsuhiko Yamaji · Teruhisa Horita · Yue-Ping Xiong · Manuel E. Brito · Harumi Yokokawa

Received: 25 April 2008 / Accepted: 15 October 2008 / Published online: 10 November 2008

Abstract The stability of yttria-stabilized zirconia (YSZ) and scandia-stabilized zirconia (ScSZ) electrolytes against boron oxide was examined. Boron oxide was painted on the polished surface of YSZ and ScSZ and annealed at 1273 K for 100 h under wet hydrogen flowing condition. The X-ray diffractometry, scanning electron microscopy/energy dispersive X-ray analysis, and Raman studies revealed that formation of Y_2O_3 and Sc_2O_3 occurred on YSZ and ScSZ surfaces contacting the boron oxide, but rare earth borates were not observed. The surface of electrolytes around precipitated particles became rough and phase transformation was confirmed from the cubic to the tetragonal or the monoclinic phases due to stabilizer removal from cubic zirconia. It has been also verified that small amounts of zirconium and yttrium were transported from the electrolyte to the gas phase via boron component. This destabilization effect induced by boron oxide was more serious for ScSZ than for YSZ. A destabilization mechanism under wet hydrogen atmosphere is proposed based on pseudo ternary phase diagrams for the $YO_{1.5}$–$BO_{1.5}$–ZrO_2 system and the $ScO_{1.5}$–$BO_{1.5}$–ZrO_2 system and thermodynamic considerations.

Introduction

Zirconium oxide (zirconia, ZrO_2) exhibits the monoclinic phase at room temperature, and with increasing temperature, it allotropically transforms to the tetragonal phase around 1200 °C and to the cubic phase around 2400 °C [1, 2]. When lower valence cations such as Y^{3+} and Sc^{3+} are doped in zirconia, the tetragonal or the cubic phase can be stabilized at lower temperatures. Those yttria (Y_2O_3)-stabilized zirconia (YSZ) and scandia (Sc_2O_3)-stabilized zirconia (ScSZ) show high oxide ion conductivity with a high ionic transport number, close to unity, over a wide oxygen partial pressure range at high temperatures [3, 4]. For these reasons, these materials are used as electrolyte materials for solid oxide fuel cells (SOFCs) [3–5]. In addition, high compatibility with other components under fabrication and during operation conditions is required for the electrolyte material [3]. In our recent investigations, the presence of impurities in SOFC stacks are more significant in the anode side than in the cathode side [6]. In the anode side, some components vaporized from the surrounding materials and were transported onto the electrolytes. To realize high durability and high reliability of SOFCs, it is important to examine the stability of electrolyte materials against other components and impurities in reducing atmosphere.

Zirconia has enough high chemical stability in SOFC operation conditions, but reactivity with sealing materials or insulators which consist of various types of oxides has not been well investigated. There are two ways of evaluating the stability of electrolyte material against minor impurities. One is the theoretical approach: evaluation of the thermodynamic compatibility. The other is performing annealing experiments where the electrolyte material is in contact with impurities. Unfortunately, there is lack in thermodynamic data for ScSZ electrolyte materials, impurities and related compounds, and, to date, there are few reports about reactions between electrolyte materials and minor impurities.

H. Kishimoto (✉) · N. Sakai · K. Yamaji · T. Horita · Y.-P. Xiong · M. E. Brito · H. Yokokawa
National Institute of Advanced Industrial Science and Technology (AIST), AIST Tsukuba Central No. 5, Higashi 1-1-1, Tsukuba, Ibaraki 305-8565, Japan
e-mail: haruo-kishimoto@aist.go.jp

Yttria-stabilized zirconia is also used for thermal barrier coating of turbine blade because of its high chemical stability and high mechanical strength at high temperatures [7]. There are some reports about stability of YSZ against vanadium oxide, an impurity found in heavy oil [8–11]. Yttrium component in the YSZ reacts with vanadium oxide to form YVO_4. As a result, yttrium is removed from YSZ and it causes the phase transformation from the cubic or the tetragonal to the monoclinic phase. It is also reported that similar destabilization processes induced by aluminum or boron component were observed for calcia-doped zirconia (CSZ) and YSZ [12–15].

Boron oxide is one of the main components of sealing glass for SOFCs, and it is in contact with electrolytes in some stack designs. Furthermore, boron component is volatile in reducing atmosphere and there exists some possibility for boron oxide to be transported from the seals to the zirconia electrolyte surface or the nickel–zirconia cermet anode surface. Boron oxide would form $(HBO_2)_3$, H_3BO_3 gaseous phases rather than gaseous B_2O_3 [16]. Consequently, it is important to clarify the reactivity between boron oxide and the electrolyte. In this study, we examine the effect of boron oxide on the stability of stabilized zirconia electrolytes under reducing atmosphere.

Experimental

The 8YSZ and 10Sc1CeSZ disks (ϕ 18 mm) were prepared from commercial powders of 8 mol% Y_2O_3-doped ZrO_2 (TZ-8Y, Tosoh Co., Japan) and 10 mol% Sc_2O_3 and 1 mol% CeO_2-doped ZrO_2 (10Sc1CeSZ, Daiichi Kigenso Kagaku Kogyo Co., Ltd., Japan), respectively. Powders were shaped into disks and pressed by cold isostatic press at 390 MPa, and then sintered at 1400 °C for 5 h in air. Surfaces of the sintered disks were polished with 1 μm diamond slurry.

Boron oxide powder (B_2O_3, Wako Pure Chemical Industries, Ltd., Japan) was dispersed in the ethanol and painted on the polished surface of 8YSZ and 10Sc1CeSZ in a circle of 5 mm in diameter. The sample disks were set in an alumina tube and treated at 1000 °C for 100 h in humidified hydrogen (about 3%) with 5 mL/min (oxygen partial pressure was calculated to be about 10^{-13} Pa).

The treated sample surface was analyzed by X-ray diffractometry (XRD, Cu-$K\alpha$, 40 kV—40 mA, RINT-UltimaIII, Rigaku Co., Japan), scanning electron microscopy (SEM, VE-7800, Keyence Co., Japan), and by energy dispersive X-ray analysis (EDX, EDAX Genesis, EDAX Japan Co., Ltd., Japan). The Raman spectra for the surface of treated samples were recorded by a Raman spectrometer (NRS-3100, JASCO Co., Japan). Laser wavelength for excitation was 532 nm and the irradiated laser power was about 10 mW. Spatial resolution was about 2 μm.

Results and discussion

After the treatment at 1000 °C for 100 h, the surface of the electrolyte where the boron oxide was painted could be recognized by naked eye because of its opacity. However, boron oxide could not be detected on that surface of electrolyte by XRD analysis. On the other hand, many needle-like crystals were found on the wall of the alumina tube near the gas exhaust. It is supposed that the most of boron oxide was vaporized, transported by gas flow, and deposited onto the wall due to the temperature gradient.

Figure 1A–D shows the SEM images for the treated 8YSZ surface. The Y/Zr ratio were determined by the semi-quantitative EDX analysis (standard-less analysis) for several points shown as e–h in Fig. 1, and the results are summarized in Table 1. At the area (A) where boron oxide was painted on the surface, facet particles (e), and plate-like particles (f) were observed, while the surface of base

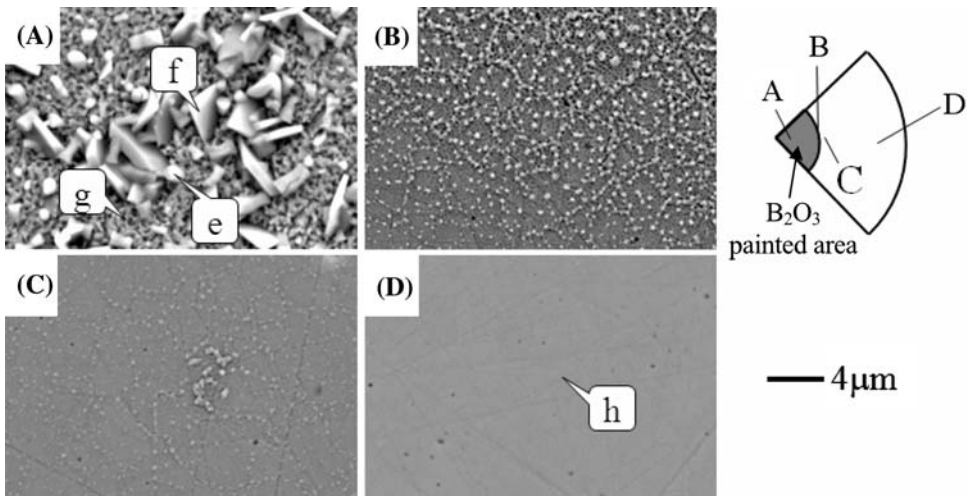

Fig. 1 SEM images for the surface of the treated 8YSZ. Schematic drawing of 1/4 piece of the 8YSZ disk was shown at upper right corner and capital letters in this drawing corresponds to the SEM images with the same letters. Small letters are EDX analyzed point summarized in Table 1

Table 1 Cation ratios on the surface of treated 8YSZ and 10Sc1CeSZ determined by results of EDX analysis with ZAF method

Measured point	8YSZ				10Sc1CeSZ				
	e	f	g	h	n	o	p	q	s
Y/Zr or Sc/Zr	1.24	0.31	0.19	0.21	1.61	0.14	1.34	1.17	0.20
Ce/Zr	–	–	–	–	0.02	0.02	0.36	0.03	0.01

Measured points shown by small letters correspond to the point shown in Figs. 1 and 2 by the same letters

Theoretical cation ratio: 8YSZ:Y/Zr = 0.17, 10Sc1CeSZ:Sc/Zr = 0.22, Ce/Zr = 0.01

8YSZ (g) became very rough. Size and number of newly crystallized particles decreased at the edge of boron oxide painted area (B), and those were much smaller at the area (C), where boron oxide was not painted. In the area (D) far from the boron oxide painted area, the surface was flat and no particles were observed. The size and number of the newly crystallized particles seems to strongly depend on the content of boron oxide painted. From the EDX analysis, it is clear that the concentration of yttrium was higher (Y/Zr = 1.24) at the precipitated particles than that at starting 8YSZ (Y/Zr = 0.21). It is obvious that yttrium in 8YSZ was removed to the surface by the presence of boron oxide, although the boron component was scarcely detected by EDX analysis for the whole area.

Scanning electron microscopy images for the surface of treated 10Sc1CeSZ are shown in Fig. 2. The Sc/Zr ratio and the Ce concentration were determined by EDX analysis for several points shown as n–s in Fig. 2, and the results are also summarized in Table 1. Large columnar particles were observed (n), and the surface of base 10Sc1CeSZ was very rough (o) in the boron oxide painted area (I). In the edge of boron oxide painted area (J), large particles were observed and the original surface of 10Sc1CeSZ became also rough. In this area, two new types of particles formed; one was facetted as shown in (p), and the other has plate-like shape (q). Rough surface was observed for 10Sc1CeSZ in a large area (areas K and L) although boron oxide was not painted in these areas. The surface near the electrolyte edge (area M) did not change by the treatment. It is clear that morphological changes of the surface occurred in a wider area for 10Sc1CeSZ than for 8YSZ. The EDX analysis revealed that the Sc concentration was much higher in the precipitated particles than that of base 10Sc1CeSZ. On the other hand, the removal of scandium was observed for the surface of the base electrolyte around the precipitated particles (point o) as shown in Table 1. Therefore, it was clear that the Sc component, which is the stabilizer of cubic zirconia phase, was removed from the base 10Sc1CeSZ to the surface in the boron oxide painted area and this change extended to the surface in the surroundings of the boron oxide painted area. Figure 3 shows the EDX maps of each component around the precipitated particles found in the boundary area (J in Fig. 2). The high Sc intensity was observed on the precipitated particles. The Ce content was different between types of particle shape, i.e., the Ce content was enriched in facetted particles, but no cerium was detected in the plate-like particles. The Ce was also removed from the base 10Sc1CeSZ and it was concentrated in facetted particles. It is noteworthy that Ce content was only 1 mol% in the starting 10Sc1CeSZ electrolyte. Even in the EDX map with high contrast, no significant distribution was observed for B.

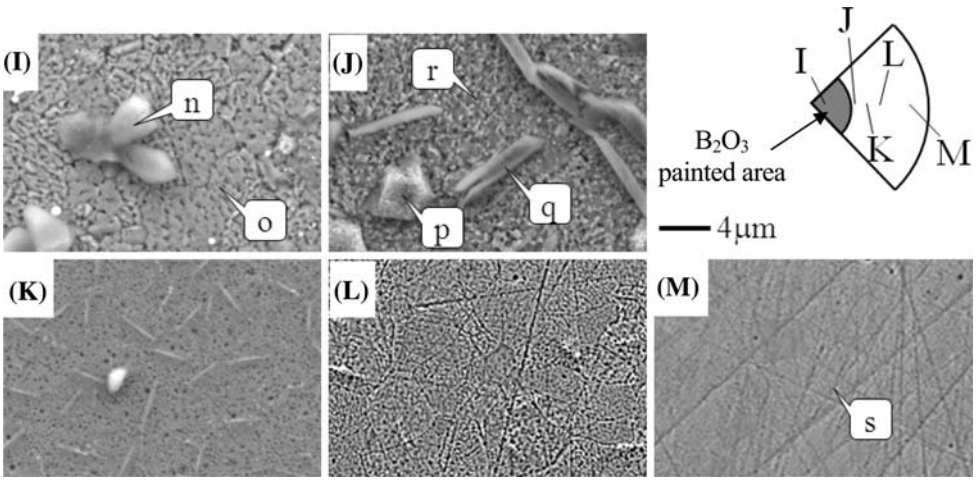

Fig. 2 SEM images for the surface of the treated 10Sc1CeSZ. Schematic drawing of 1/4 piece of the 10Sc1CeSZ disk was shown at upper right corner and capital letters in this drawing corresponds to the SEM images with the same letters. Small letters are EDX analyzed point summarized in Table 1

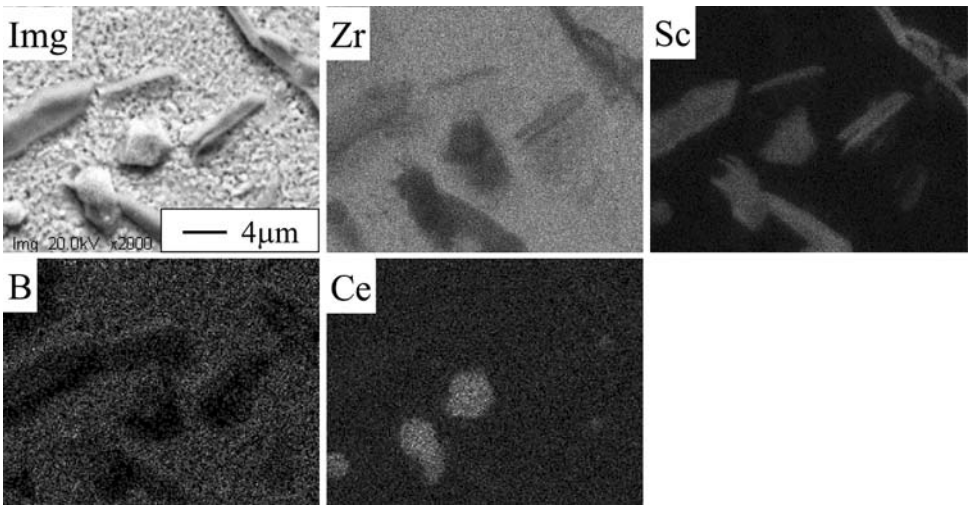

Fig. 3 Mapping results of EDX analysis for the treated 10Sc1CeSZ surface. This area corresponds to the boundary area of (F) in Fig. 2

The Raman spectra were collected for the points indicated in Fig. 2n–r and the results were shown in Fig. 4. The spectrum corresponding to single C-rare earth type Sc_2O_3 is also presented for the sake of comparison. The spectrum for the particle (n) essentially corresponds to the Sc_2O_3 with C-rare earth structure, and it also contains very small peaks from monoclinic zirconia [17]. The particle was identified as Sc_2O_3. The surface (o) was identified as monoclinic zirconia [17] even though the peaks were slightly broadened. Raman spectrum for the particle (p) shows the mixture of Sc_2O_3 and monoclinic zirconia. The particle (q) consisted of Sc_2O_3 and cubic zirconia [17]. The 10Sc1CeSZ surface pointed by (r) was identified as monoclinic zirconia. In the Raman spectra for o–r, very small peaks from the tetragonal zirconia [17] were also observed. These results suggest that 10Sc1CeSZ transformed from cubic to monoclinic and tetragonal phases. The surface not being affected by boron oxide (s) was identified as cubic zirconia by that Raman spectrum. The result of Raman mapping analysis about the intensity for typical peak of each phase is shown in Fig. 5. The analyzed area was the area (I) in Fig. 2 and typical peaks were selected as 405–430 cm^{-1} for Sc_2O_3, 460–487 cm^{-1} for monoclinic zirconia, 245–275 cm^{-1} for tetragonal zirconia, and 530–685 cm^{-1} for all zirconia phases. The particles formed were identified as Sc_2O_3 and this phase was not detected in other areas. The formation of monoclinic zirconia was observed around the formed particles. It is clear that the treatment with B_2O_3 in reducing atmosphere at 1000 °C gives rise to the removal of scandium and cerium from 10Sc1CeSZ which results in the formation of particles like Sc_2O_3 and the phase transformation of zirconia from cubic to monoclinic phase.

Finally, Fig. 6 shows the result of SEM/EDX analysis for needle-like crystals deposited on the low temperature

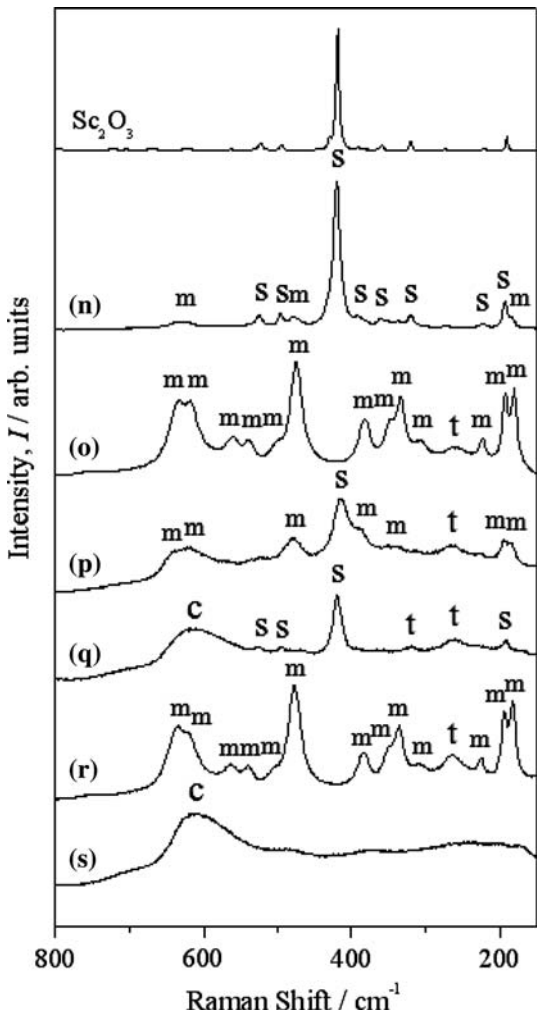

Fig. 4 Raman spectra for the surface of the treated 10Sc1CeSZ. Spectra were obtained for the points shown in Fig. 2e–j and compared with that of commercial Sc_2O_3. s: Sc_2O_3, m: monoclinic zirconia, t: tetragonal zirconia, and c: cubic zirconia, respectively

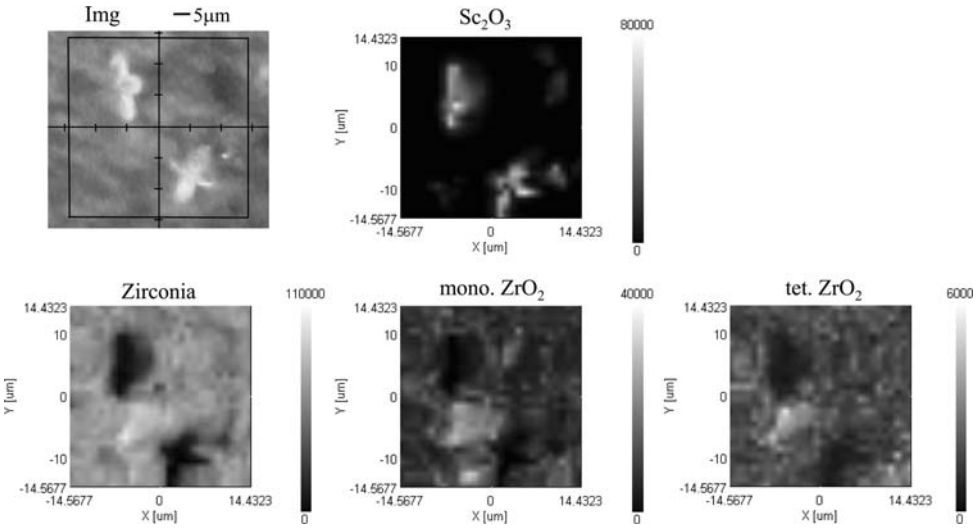

Fig. 5 Mapping result of Raman intensity for the treated 10Sc1CeSZ surface. This area corresponds to the area E in Fig. 2. Typical peak was selected as 405–430 cm^{-1} for Sc_2O_3, 460–487 cm^{-1} for monoclinic zirconia, 245–275 cm^{-1} for tetragonal zirconia, and 530–685 cm^{-1} for all zirconia phases, respectively

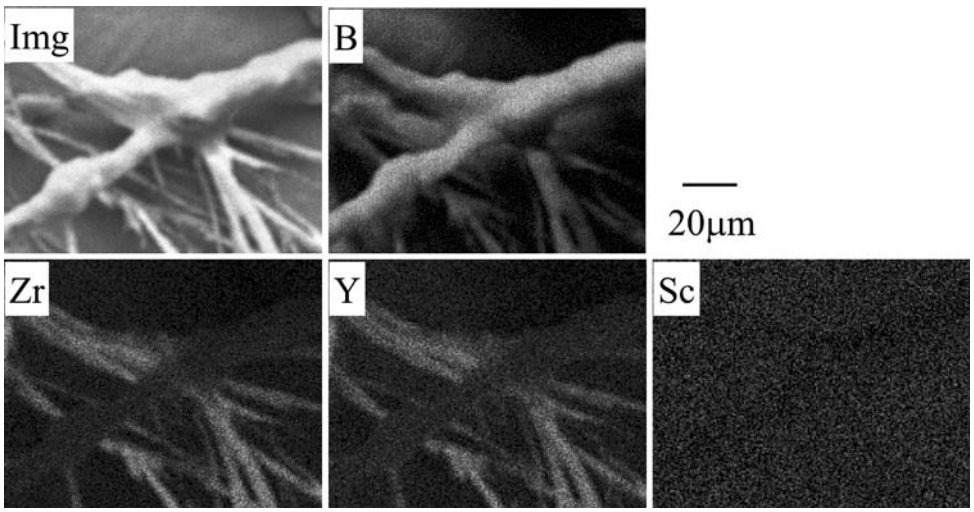

Fig. 6 Mapping results of EDX analysis for needle-like crystals precipitated on the low temperature part of alumina tube for the exhaust side

part of alumina tube close to the exhaust side. The needle-like crystals consisted of thick trunk and thin branches as revealed in the SEM image. Boron was detected in both trunk and branches. At the branches, yttrium and zirconium were also detected, but scandium was not. It is suggested that yttrium and zirconium were reacted with boron oxide and transported to the low temperature part via gaseous phases.

To explain the present observations, it is needed to summarize the earlier information on reactions or phase relations:

(1) When boron oxide alone is heated, boron oxide is melted about 450 °C [18, 19]. Chemical equilibrium calculations were made to know the major gaseous species in the present heat treatment with thermodynamic database MALT/gem [16], and results suggest that gaseous species of HBO_2 and $(HBO_2)_3$ are dominant and have the partial pressure in the order of 10^{-4}–10^{-5} atm. Thus, in the present case, it is suggested that boron oxide on the zirconia electrolytes melted during heating process, and gradually and eventually all boron oxide was volatilized from the electrolyte surface during the annealing at 1000 °C for 100 h.

(2) There are some reports about destabilization mechanism of stabilized zirconia in the presence of boron oxide [12, 14, 15]. The reported destabilization mechanism is described by the following reactions:

$$B_2O_3 + Y_2O_3(\text{in YSZ}) \Rightarrow 2YBO_3 + m\text{-}ZrO_2 \quad (1)$$

$$B_2O_3 + Sc_2O_3(\text{in ScSZ}) \Rightarrow 2ScBO_3 + m\text{-}ZrO_2 \quad (2)$$

Stabilizer of Y and Sc is removed from the stabilized zirconia by the formation of rare earth borates.

(3) Figure 7 summarizes the available information on pseudo-ternary phase diagrams for (a) $YO_{1.5}$–$BO_{1.5}$–ZrO_2 system and (b) $ScO_{1.5}$–$BO_{1.5}$–ZrO_2 system at 1273 K estimated from references [18–20]. The phase

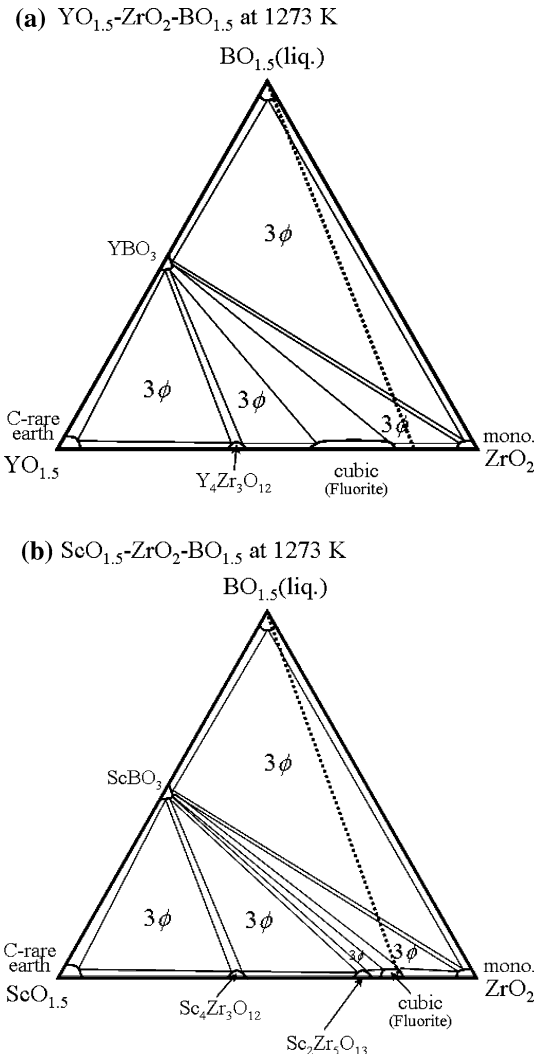

Fig. 7 Schematic drawings of possible pseudo ternary phase diagrams for **a** $YO_{1.5}$–$BO_{1.5}$–ZrO_2 system and **b** $ScO_{1.5}$–$BO_{1.5}$–ZrO_2 system at 1273 K. The single-phase regions were exaggerated in these figures. Phase diagrams for $YO_{1.5}$–ZrO_2 system and $ScO_{1.5}$–ZrO_2 system were referred from [19] and those for $YO_{1.5}$–$BO_{1.5}$ and $ScO_{1.5}$–$BO_{1.5}$ were referred from [17] and [18]. Dashed lines in (a) and (b) shows the composition pass between 8YSZ and $BO_{1.5}$ and between 10Sc1CeSZ and $BO_{1.5}$, respectively. 3ϕ in these phase diagrams show three phase equilibrium regions

diagrams only show the equilibrium state among the condensed phases, and considerations on gaseous species are needed to complement the relations under reducing condition. This phase relation in the B_2O_3-rich corner is consistent with the earlier observation of destabilization of YSZ or ScSZ (Eqs. 1 and 2). The reaction products are in equilibrium with each other. Since one of the major reactants is in liquid state, the reaction may proceed by dissolution of YSZ (ScSZ) into the liquid and precipitation as *m*-ZrO_2 and YBO_3 ($ScBO_3$).

On the basis of these earlier results, the followings are the main points to be considered:

(i) In the present results, boron was not detected at the formed particles rich in Y or Sc according to EDX analysis, and boron oxide and borates were detected neither by XRD nor by Raman spectroscopy. Why are Y_2O_3 or Sc_2O_3 formed instead of YBO_3 or $ScBO_3$? It is noteworthy that these oxides are not in equilibrium with other reactants and products except for YBO_3 and $ScBO_3$.

(ii) Mass transportation via gas phase involves only Y and Zr but not Sc, whereas destabilization reactions take place in a more significant manner on 10Sc1CeSZ. How do these differences arise?

To consistently explain the above features, we propose the following mechanism consisting of several different reaction steps as follows:

1. Boron oxide melted on the electrolyte surface. This is a fast process that it is accomplished during heating process.
2. The reactions occurred between the B_2O_3(liq.) and the 8YSZ or the 10Sc1CeSZ, and as a result, rare earth borates and monoclinic ZrO_2 (*m*-ZrO_2) were formed according to the phase diagrams:

$$YSZ + B_2O_3(liq.) \Rightarrow YBO_3 + m\text{-}ZrO_2 \quad (3)$$

$$ScSZ + B_2O_3(liq.) \Rightarrow ScBO_3 + m\text{-}ZrO_2 \quad (4)$$

   In this reaction process, particle growth of *m*-ZrO_2 and rare earth borates may proceed by dissolution and reprecipitation process of Zr, Y, and Sc components in electrolytes with the B_2O_3(liq.). It is also clear from the phase diagrams that rare earth oxide (Ln_2O_3, Ln = rare earth metals) is not directly formed from the reaction of stabilized zirconia with B_2O_3(liq.).
3. YBO_3 and $ScBO_3$ have high melting points of about 1600 °C [18, 19] and eutectic points between borates and B_2O_3(liq.) are as high as 1373 and 1526 °C for YBO_3 and $ScBO_3$, respectively [18, 19]. In addition, from the phase diagram, it is suggested that borates can exist with high boron activity (co-existence of borates and B_2O_3(liq.)). Decomposition of borates is commenced after B_2O_3(liq.) is diminished by volatilization and transportation from the electrolyte surface.
4. Two phase equilibrium between borates and rare earth oxides become stable when boron activity is decreased. The borates may be decomposed into rare earth oxides by the following equations under wet hydrogen condition:

$$2YBO_3 + H_2O \Rightarrow Y_2O_3 + 2/3(HBO_2)_3(gas) \quad (5)$$

$$2ScBO_3 + H_2O \Rightarrow Sc_2O_3 + 2/3(HBO_2)_3(gas) \quad (6)$$

Under wet hydrogen condition, $(HBO_2)_3$(gas) is stable, as mentioned above, and, therefore, these reactions cannot proceed under dry or oxidation conditions. The formed $(HBO_2)_3$(gas) is then transported from the reaction site because of the gas flow. This reaction proceeds until borates are completely decomposed. The precursor of the rare earth oxide, that is the borate, may be formed in large and well-crystallized particles by dissolution and reprecipitation process (proposed step 2) and the resulting rare earth oxides may be also well-crystallized particles.

Particle precipitation and rough surface were observed where boron oxide was not painted (area G and H in Fig. 2); this is more serious for 10Sc1CeSZ electrolyte than that for 8YSZ electrolyte. This may occur via diffusion through the liquid B_2O_3. It is suggested that reactivity of 10Sc1CeSZ with B_2O_3(liq.), in other words, dissolution of rare earth metals and zirconium into liquid phase, is higher than that of 8YSZ. In the present results, yttrium and zirconium were detected with boron oxide at the low temperature part of the alumina tube via gas phase but scandium was not, although reactivity of 10Sc1CeSZ with B_2O_3 should be higher. Volatilization reactions of yttrium and scandium can take place by assuming the existence of YBO_2(gas) and $ScBO_2$(gas) phases; for the B_2O_3–Al_2O_3 system, gaseous $AlBO_2$ formation is suggested under the reducing condition [16].

$$\text{Y in } B_2O_3(\text{liq.}) + H_2 \Rightarrow YBO_2(\text{gas}) + H_2O \quad (7)$$

$$YBO_3 + H_2 \Rightarrow YBO_2(\text{gas}) + H_2O \quad (8)$$

$$\text{Sc in } B_2O_3(\text{liq.}) + H_2 \Rightarrow ScBO_2(\text{gas}) + H_2O \quad (9)$$

$$ScBO_3 + H_2 \Rightarrow ScBO_2(\text{gas}) + H_2O \quad (10)$$

The difference in volatilized rate between yttrium and scandium may be due to the stability of gas $LnBO_2$ (Ln: rare earth metals). As for the 10Sc1CeSZ, $ScBO_2$(gas) may be less stable and, even when $ScBO_2$(gas) was formed, this gaseous phase would be immediately decomposed into other phases according the following reaction:

$$2ScBO_2(g) + 3H_2O \Rightarrow Sc_2O_3 + 2/3(HBO_2)_3(g) + 2H_2 \quad (11)$$

Zirconium was also transported via gas phase. One possibility is volatilized with B_2O_3(liq) and the other is the formation of gaseous $Zr(OH)_4$ under wet-reducing condition in an analogous way to $Si(OH)_4$. However, we have no more experimental evidence for this phenomenon. A comprehensive explanation of the destabilization process has to include the reaction related to zirconium with gaseous phases. Needless to say that the destabilization processes can proceed not only according to thermodynamic equilibria, but also we have to take into account nonequilibrium conditions and kinetics considerations.

As we have already mentioned in the introduction, boron oxide is often contained in sealing materials for SOFCs. The present experimental results revealed that boron components greatly affect the zirconia electrolyte stability in a reducing atmosphere. It is expected that the destabilization leads to lowering oxide ion conductivity of the electrolyte and changes of thermal expansion coefficient induced by phase transformation from the cubic to the tetragonal or the monoclinic phases. Especially for the SOFCs with thin film zirconia electrolyte, thermal expansion changes in the electrolyte film will cause mechanical instability such as crack formation. When attention is paid on the stabilizer, the formation of double oxides with acidic oxides such as vanadium oxide and boron oxide can be regarded as the driving forces for destabilization of stabilized zirconia. In the present investigation, a more interesting phenomenon was observed; that is, such a double oxides can be decomposed into the constituent oxides, namely, Y_2O_3 or Sc_2O_3. These oxides are quite basic and therefore their reactivity with other impurities should be quite high. A major finding is that it is important to avoid the contact between the zirconia electrolyte and boron containing glass sealing materials used in the fuel side.

In summary, the destabilization of zirconia electrolyte induced by the contact with boron oxide was experimentally observed. A new feature of the destabilization mechanism that incorporates reaction with gaseous species was proposed. It is also suggested that stability of all SOFC components under the SOFC operating condition must be examined. In future works, we will further examine the effect of impurities and contaminants, boron oxide on electrolyte materials and electrode materials, and we will clarify the degradation mechanism by combining both experimental and thermodynamic considerations.

Conclusion

In the present study, destabilization of 8YSZ and 10Sc1CeSZ electrolytes induced by boron oxide was examined by SEM/EDX and Raman spectroscopy. Stabilizers, Y and Sc, were removed from 8YSZ and 10Sc1CeSZ by reaction with liquid boron oxide, respectively, and correspondingly Y_2O_3 and Sc_2O_3 were formed on the surface of 8YSZ and 10Sc1CeSZ. As a result, the surface of zirconia transformed to tetragonal or monoclinic phase around formed particles. A part of yttrium and zirconium was transported away from electrolyte via gaseous phases. The

destabilization effect of boron oxide is more critical for 10Sc1CeSZ than that for 8YSZ. A new destabilization mechanism with formation and decomposition of rare earth borates under the wet hydrogen atmosphere is proposed.

Acknowledgement This study was supported by the New Energy and Industrial Technology Development Organization (NEDO) of Japan.

References

1. Abriata JP, Garces J, Versaci R (1986) Bull Alloy Phase Diagr 7:116
2. Wang WE, Olander DR (1993) J Nucl Mater 201:231
3. Minh NQ, Takahashi T (1995) In: Science and technology of ceramic fuel cells. Elsevier, Amsterdam, p 69
4. Ishihara T, Sammes NM, Yamamoto O (2003) In: Singhal SC, Kendall K (eds) High temperature solid oxide fuel cells—fundamentals, design and applications. Elsevier, Oxford, p 83
5. Mizutani Y, Tamura M, Kawai M, Yamamoto O (1994) Solid State Ion 72:271
6. Yokokawa H, Horita T, Yamaji K, Kishimoto H, Xiong YP, Brito ME (2008) In: Steinberger-Wilckens R (ed) Proceedings of 8th European solid oxide fuel cell forum, B1004
7. Toriz FC, Thakker AB, Gupta SK (1989) Surf Coat Technol 39/40:161
8. Susnitzky DW, Hertl W, Barry Carter C (1988) J Am Ceram Soc 71:992
9. Hertl W (1988) J Appl Phys 63:5514
10. Jones RL (1990) High Temp Sci 27:369
11. Yokokawa H, Sakai N, Kawada T, Dokiya M (1993) In: Badwal SPS, Bannister MJ, Hannink RHJ (eds) Science and technology of zirconia V. The Tenomic Publication Co. Inc., Lancaster, PA, USA, p 752
12. Buchanan RC, Sircar A (1983) Comm Am Ceram Soc Feb:C-20
13. Ananthapadmanabhan PV, Menon SB, Venkatramani N, Rohatgi VK (1989) J Mater Sci 24:4432
14. Guo X (1996) J Mater Sci Lett 15:38
15. de Florio DZ, Muccillo R (2004) Mater Res Bull 39:1539
16. Calculated with the thermodynamic database MALT for windows and the programs *gem* and *CHD*, Kagaku gijutsu-Sha, Japan. http://ww.kagaku.com/malt/
17. Fujimori H, Yashima M, Kakihana M, Yoshimura M (1998) J Am Ceram Soc 81:2885
18. Levin EM (1967) J Am Ceram Soc 50:53
19. Figure 4390 (1975) In: Levin EM, McMurdie HF (eds) Phase diagrams for ceramists. The American Ceramic Society, Inc., p 140
20. Yokokawa H, Sakai N, Kawada T, Dokiya M (1993) In: Badwal SPS, Bannister MJ, Hannink RHJ (eds) Science and technology of zirconia V. Tenomic Publication Co. Inc., Lancaster, PA, USA, p 592